ACS OMEGA

Open Access

http://pubs.acs.org/journal/acsodf

Article

Shape-Specific Gold Nanoparticles for Multiplex Biosensing Applications

Shixi Zhang, Yuhan Zhang, Jiaye Jiang, Mathias Charconnet, Yuan Peng, Lei Zhang,* and Charles H. Lawrie*

Cite This: *ACS Omega* 2024, 9, 37163−37169

Read Online

ACCESS | Metrics & More | Article Recommendations | Supporting Information

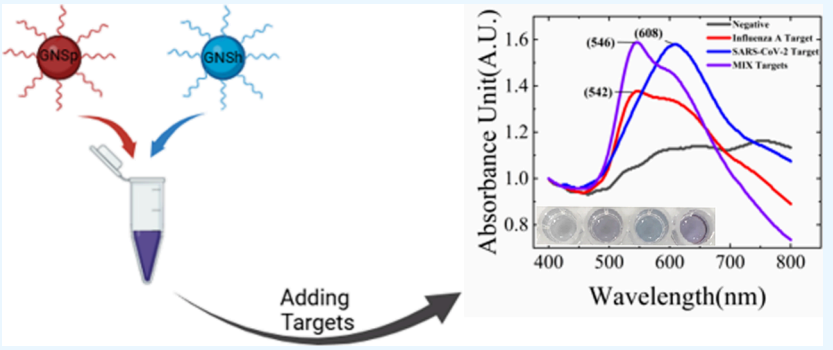

ABSTRACT: The biosensing field faces a significant challenge in efficiently detecting multiple analytes in a single diagnostic sample in order to compete with other established multiplex molecular diagnostic technologies such as PCR and ELISA. In response, we have developed a colorimetric nanobiosensor based on multiple morphological forms of functionalized gold nanoparticles (AuNPs) for the simultaneous detection of the influenza virus and SARS-CoV-2 virus. Gold nanospheres (GNSp) were modified with oligonucleotides specific for the influenza A virus, while gold nanoshells (GNSh) were modified with oligonucleotides specific for the SARS-CoV-2 virus. In the presence of their respective targets, AuNPs remain stable due to DNA−DNA interactions; conversely, in the absence of targets, AuNPs aggregate. Consequently, the hybrid system exhibits an indigo color with the SARS-CoV-2 target, a blue color with the Influenza A target, and a purple color with both targets, visible to the naked eye. Analytical sensitivity was 100 nM, and no cross-reactivity was observed with potentially confounding pathogens. This approach holds great promise for the simultaneous identification of multiple pathogens in a rapid manner without the need for equipment or trained personnel.

INTRODUCTION

Biosensors have attracted widespread attention from the scientific community due to their wide range of applications.[1,2] Capable of performing both qualitative and quantitative analyses of biological components through detectable signals, biosensors have become indispensable tools in the recognition of harmful viruses,[3] bacteria,[4] and fungi[5] or for monitoring levels of metabolites in the human body using wearable sensors for instance.[6] Ever since the invention of biosensors designed for quantifying glucose in biological samples,[7] the widespread adoption of biosensors extends across various domains, including food,[8−10] biomedicine,[11−13] environmental monitoring,[14−16] drug development, and numerous other fields.

In particular, different clinically relevant techniques have been developed to detect DNA, RNA, antigens, or antibodies acting as biomarkers of viruses, bacteria, or fungi. Molecular diagnosis (i.e., nucleic acid detection) remains the gold standard of infectious disease diagnostics, and PCR is the most widely used technique for molecular diagnostics. However, PCR is expensive, has a long turnaround time, and requires centralized laboratories, specialized equipment, and trained personnel, which makes it unsuitable for resource limited settings.[17] Loop isolated mediated amplification (LAMP) is an emerging alternative molecular diagnostic technology to PCR; however, it also has a relatively high cost, is enzyme-based, and needs the isolation of DNA/RNA.[18] More recently, new molecular techniques such as CRISPR are being used for precise biosensing by coupling them with visual readout using gold NPs[19] or electrochemical sensing.[20]

Nanotechnology has enabled the fabrication of new biosensors based on the use of nanoparticles of different materials that offer alternatives to enzyme base amplification molecular diagnostic systems such as PCR and LAMP.[21,22]

Received: May 8, 2024
Revised: July 18, 2024
Accepted: July 24, 2024
Published: August 19, 2024

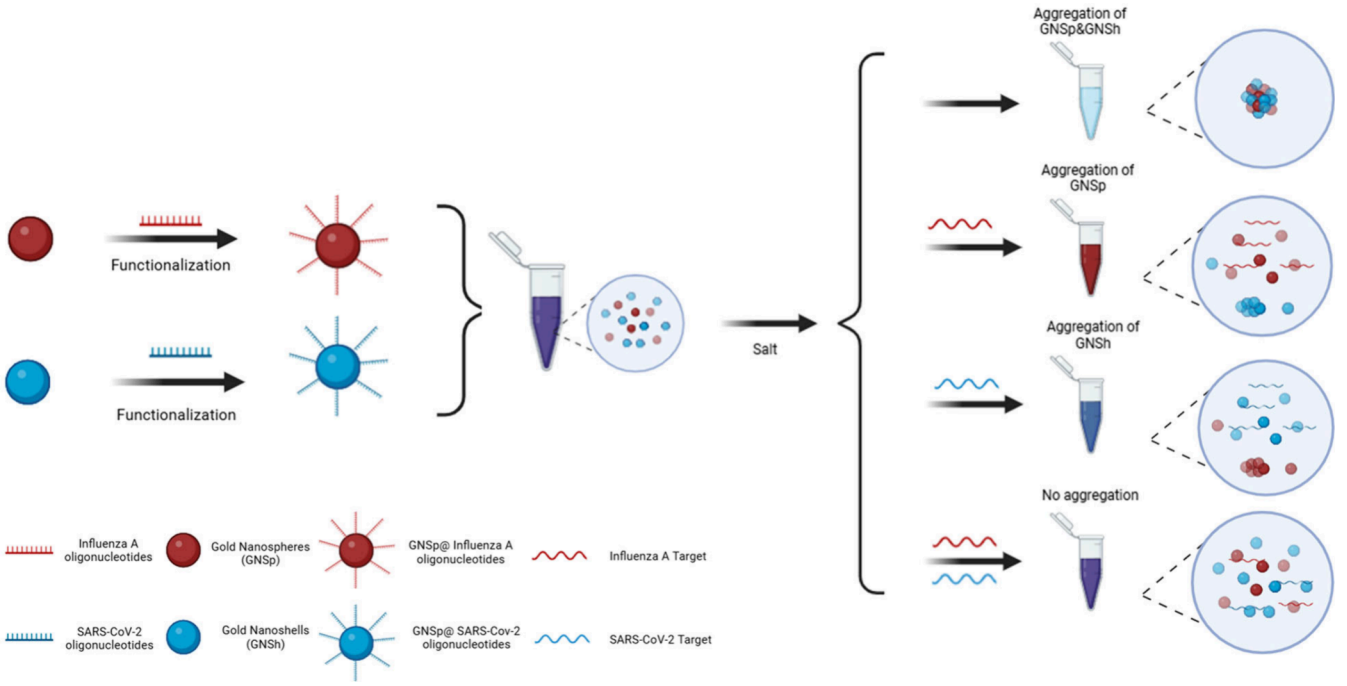

Figure 1. Schematic diagram of multiple analyte detection based on different forms of gold nanoparticles.

Certainly, owing to their remarkable optical and electrical properties, functionalized gold nanoparticles can transduce molecular binding events, such as DNA/DNA, DNA/RNA, or antibody/antigen interactions. The detection readout of these colloidal biosensors can be detected through visual observation, colorimetric changes, or electrical signals. Gao et al. designed a novel labeling free adaptive sensor for colorimetric determination of small molecules.[23] Under salt-induced conditions, the target formed a double-stranded structure with the hairpin DNA, causing the unmodified gold nanoparticles to aggregate when exposed to the solution, leading to a change in the red-to-blue color. As an example of electrochemical readout, Zeng et al. used antibody labeled gold NPs as the electrode coupled to a smartphone for electrochemical readout to sense nucleocapsid proteins from SARS-COV2.[24] Finally, lateral flow assays (LFA) employing gold nanoparticles are frequently used for detecting antibodies or antigens and provide a visual readout. Additionally, LFAs can be used to detect nucleic acids using biotinylated oligonucleotides.[25] Recent advances in biosensing systems have led to the development of novel gold nanoparticle biosensors based on colorimetric changes in solution. These innovations are garnering interest as potential alternatives to LFAs methodologies, which can suffer from low sensitivity.[25−28] Typically, these assays rely on oligonucleotide-functionalized gold nanoparticles that can be used to detect a wide range of microorganisms.[29] Moreover, they offer a user-friendly and rapid detection platform, demonstrating promising potential for widespread applications.[29] However, to date, these biosensors have been limited to detecting a single pathogen/analyte.

The capacity to concurrently detect multiple pathogens in a single reaction (**MULTIPLEXING**) is becoming increasingly prevalent in diagnostic technologies. Multiplexed PCR, a well-established technique, has been commercially available with kits designed for the detection of sexually transmitted diseases offered by numerous manufacturers.[30] More recently, multiplexed lateral flow assays have emerged and are now being marketed for the simultaneous identification of influenza A, influenza B, and SARS-CoV-2.[31] Some assays integrating LFA with PCR/LAMP have demonstrated multiplexed detection of sexually transmitted diseases.[32] Below we describe a system based on different morphologies of gold nanoparticles to simultaneously detect multiple pathogens providing multiplex ability to the colloidal biosensor system in a simple-to-use, economic, point-of-contact (POC) format direct from the sample to visual output visible to the naked eye (Figure 1).

EXPERIMENTAL SECTION

Materials and Characterization. Ultrahigh concentration colloidal gold nanoparticles (AuNPs; 60 nm, 100 OD) were acquired from Zhengzhou Lingsi Bio-Tech Co., Ltd. Sodium citrate-modified GNSh was obtained from Zhongkekeyou. Sodium dodecyl sulfate (SDS), sodium citrate tribasic dihydrate, and Triton X-100 were sourced from Sigma-Aldrich. Ethylene diamine tetraacetic acid (EDTA, 0.5 M, pH = 8.0) and TRIS hydrochloride were procured from Thermo Fisher Scientific Inc. Phosphate buffer solution (1.0 M, pH = 7.4) was purchased from Aladdin. Proteinase K was acquired from Beyotime Biotechnology. Sodium chloride was obtained from Sinopharm Chemical Reagent Co., Ltd. Custom-made oligonucleotides (ssDNAs) functionalized with thiol moieties at the 5′ end were purchased from Generay biotech. UltraPure DNase/RNase-Free Distilled Water was obtained from Thermo Fisher Scientific Inc. Custom oligonucleotides (100 μM) were diluted with UltraPure DNase/RNase-Free Distilled Water. All other reagents were prepared by using Milli-Q water. The UV−visible spectra of AuNPs were measured by using a dual-beam UV−visible spectrophotometer (Beijing General Analytical Instruments). The hydrodynamic diameter and zeta potential of AuNPs were determined by using a dynamic light scatterer (Opptronix Technology Shanghai Ltd.). The UV−visible spectra of the AuNPs-based assay were recorded with a Plate Reader (ThermoFisher Multiskan

https://doi.org/10.1021/acsomega.4c04385
ACS Omega 2024, 9, 37163−37169

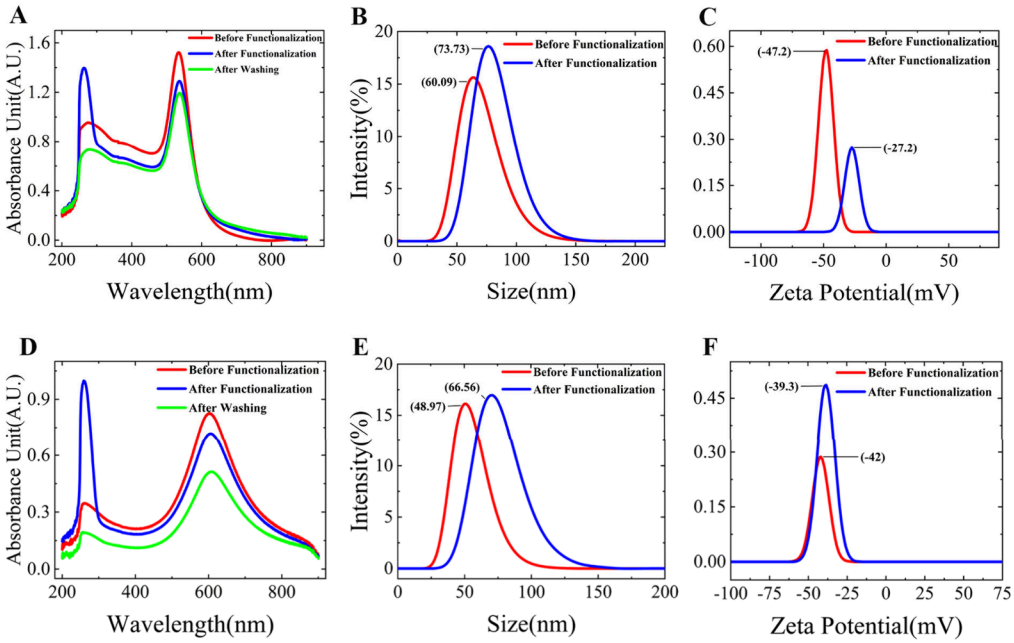

Figure 2. Ultraviolet scanning spectra and dynamic light scattering of GNSp (A–C) and GNSh (D–F). (A) Changes in ultraviolet scanning spectra during the synthesis of oligonucleotide-capped GNSp. (B) Particle size change of GNSp. (C) Zeta potential change of GNSp. (D) Changes in ultraviolet scanning spectra during the synthesis of oligonucleotide-capped GNSh. (E) Particle size change of GNSh. (F) Zeta potential change of GNSh.

SkyHigh). Transmission electron microscopy (TEM) images were taken using a fei talos120c microscope from Thermo Fisher Scientific China.

Functionalization of AuNPs with ssDNA. Gold nanospheres (GNSp) were diluted from 100 to 1.5 OD by using sodium citrate. For gold nanoshells (GNSh), the purchased solution was utilized as provided (0.05 mg/mL). Sodium dodecyl sulfate (SDS, 0.1%) and phosphate buffer (PB, 1 M, pH = 7.4) were introduced to the solution, with concentrations of SDS and PB adjusted to 0.0055% and 0.0055 M, respectively. Subsequently, oligonucleotides (refer to Table S1 for GNSp and Table S2 for GNSh, in Supporting Information (SI)) were incorporated into the solution, and the concentration was adjusted to 2 μM. Oligonucleotides corresponding to the influenza A virus were added to the solution of GNSp, while those corresponding to SARS-CoV-2 were added to the solution of GNSh. Subsequently, the oligonucleotide/AuNPs solution was placed on a shaker at room temperature for 15 min. The concentration of NaCl was increased to 0.005 M using 2 M NaCl without altering the concentrations of SDS and PB, in order to increase the oligonucleotide density on the NP.

The oligonucleotide/AuNPs solution underwent sonication for approximately 20 s, followed by a 15 min incubation period at room temperature. This procedure was iterated with increments of 0.005 0.015, 0.025, and 0.05 M NaCl until reaching a concentration of 0.1 M NaCl. The salting process was concluded with an overnight incubation at room temperature.

To eliminate excess oligonucleotides, the AuNPs were centrifuged, and the supernatant was carefully removed. The solution of GNSp underwent centrifugation at 2000 g for 40 min, while the solution of GNSh was centrifuged at 3500 g for 20 min. Following the removal of the supernatant, the AuNPs solution was subjected to two cleaning cycles using 0.01% SDS at the respective speed and time. Consequently, TE buffer 1X (Tris 0.01 M, pH = 8, EDTA 0.001 M) was introduced to the solution, and measurements were conducted by using a UV spectrophotometer and dynamic light scatterer. After another round of centrifugation, the supernatant was removed, and the concentration of GNSp was adjusted to 15 OD, while the concentration of GNSh was set to 1 mg/mL by using TE buffer.

120-nt Synthetic Target Detection. In a typical detection experiment, 46.5 μL of stock solution (SDS 0.1%, Triton X-100 0.1%, and Proteinase K 0.54 mg/mL) and 8.5 μL of functionalized AuNPs were added to a 96-well plate and mixed well by shaking. Then, 1 μL of water was added to the negative control group, and 1 μL of target at the concentration of 1 μM was added to the positive control group. Finally, a NaCl (5 M) solution was added to the mixture in desired volume. The optimal salt concentration for different types of nanoparticles was found by varying the amount of NaCl (5 M) added to a detection experiment. UV–vis spectra were then recorded at different waiting times using a microplate reader. DLS measurements of the NPs in the presence or absence of short target were also recorded by diluting 10 μL of the AuNPs into 990 μL of water.

The limit of detection (LOD) was determined by assessing serially diluted short targets under the optimal salt concentration conditions outlined for the hybrid systems.

GNSp and GNSh were combined in equal proportions within a 96-well plate to observe the color changes monitored by UV–vis spectroscopy. The hybrid systems underwent the same detection experiments as described previously, except that each test well received 8.5 μL of GNSp and 8.5 uL of GNSh. Optimal NaCl concentration was determined for both GNSp and GNSh of 0.924 and 1.267 M, respectively, for the hybrid system.

https://doi.org/10.1021/acsomega.4c04385
ACS Omega 2024, 9, 37163–37169

RESULTS

Design of Oligonucleotides for the Detection of SARS-COV-2 and Influenza A. Oligonucleotides targeting SARS-CoV-2 were sourced from our prior investigation.[33] Specifically, 20-nucleotide sequences were crafted to identify the envelope protein region on the viral RNA of SARS-CoV-2 called the *enveloped gene* (E gene). The selection of the E gene was based on its propensity for minimal mutation rates across various viral variants.[34−36]

For influenza A, the oligonucleotides were designed to detect the region encoding protein 1 of the *matrix gene* (M gene), a target commonly used for PCR detection of influenza A.

Binding energy to target, secondary structure energy, and self-binding energy were calculated for all the possible oligonucleotides present on the E gene of SARS-CoV-2 and on the M gene of influenza A using viennaRNA 2.5.[33] The oligonucleotides were selected to maximize binding energy, minimize self-binding energy, and avoid secondary structure formation. Sequences of the designed oligonucleotides can be found in the Supporting Information (Table S1).

Synthesis of AuNPs Capped with Designed Oligonucleotides. The designed oligonucleotides were utilized to functionalize citrate-stabilized gold nanospheres (GNSp) and gold nanoshells (GNSh) by binding the thiol group, located at the 5′ end of the oligonucleotides, to the gold surface. While GNSp were functionalized with oligonucleotides targeting influenza A, GNSh were functionalized with oligonucleotides targeting SARS-CoV-2 (Figure 1). Confirmation of the formation of single-stranded DNA (ssDNA)-conjugated AuNPs was achieved through various characterization techniques, including UV−vis absorbance spectroscopy and dynamic light scattering (DLS).

Prior to functionalization, GNSp displayed an absorption peak at 536 nm and GNSh displayed an absorption peak at 615 nm due to their respective plasmon resonance. After functionalization, the plasmon resonance of GNSp and GNSh shifted by 2 nm (see Figure 2A and 2D), indicating successful oligonucleotide binding to the nanoparticles. Additionally, an absorption peak was observed at 262 nm, attributable to the presence of unbound ssDNA in solution, which disappeared after the nanoparticles were washed to remove excess oligonucleotides. Further characterization of the ssDNA-stabilized AuNPs was conducted by using DLS. Figures 2B (GNSp) and 2E (GNSh) illustrate the increase in the average size of AuNPs after functionalization, confirming the formation of ssDNA-conjugated thiol-stabilized AuNPs. The increase in the electric potential, resulting from the removal of negatively charged citrate molecules from the gold nanoparticle surface, further supports their formation (Figure 2C for GNSp and Figure 2F for GNSh).

Viral Short Target Sequences Analysis Based on Single AuNP. The stability of the NPs was assessed through UV−vis spectroscopy. In the presence of their respective synthetic targets, the NPs remained stable, as indicated by the consistent absorption peaks at 538 nm for GNSp and 616 nm for GNSh due to their respective plasmon resonance. Conversely, in the absence of the short targets, NP aggregation occurred, resulting in weakened and broadened absorption peaks, along with increased absorption toward longer wavelengths due to plasmon resonance coupling in gold NP aggregates (see Figure 3B,D). This phenomenon demonstrates

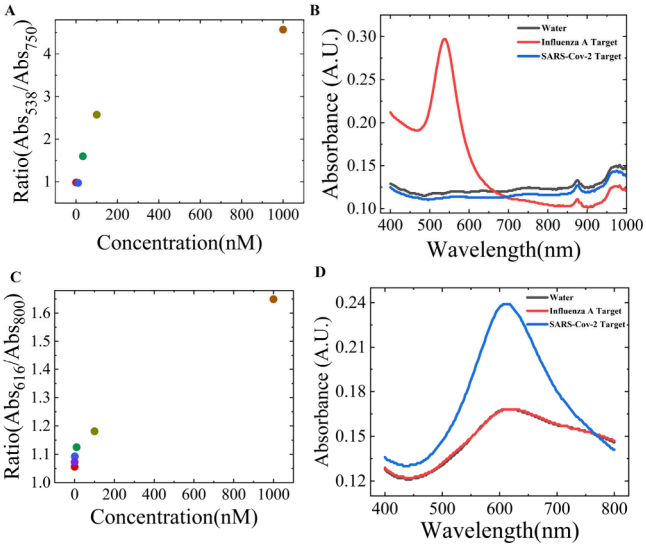

Figure 3. Sensitivity study based on AuNPs analysis: (A) LOD analysis of GNSp (water, 10, 33, 100, and 1000 nM; ratio = Abs_{538}/Abs_{750}). (C) LOD analysis of GNSh (water, 0.1, 1, 10, 100, and 1000 nM; ratio = Abs_{616}/Abs_{800}). Specificity study was based on the (B) Influenza A detection spectrum by GNSp and (D) SARS-CoV-2 detection spectrum by GNSh.

the stability of the AuNPs against salt-induced aggregation when hybridized with their complementary targets, while aggregation occurs in the absence of targets due to reduced electrostatic repulsion conferred by the presence of oligonucleotides on the surface of the AuNPs.

The absorption characteristics of the AuNP aggregates allowed monitoring the aggregation state by calculating absorption ratios at specific wavelengths Abs (538 nm)/Abs (750 nm) for the GNSp and Abs (616 nm)/Abs (800 nm) for the GNSh. Optimal salt concentrations were determined through series of experiments to obtain the maximum difference in absorption ratios between negative controls and synthetic target detection for both GNSp and GNSh and the effect of salt on the aggregation of functionalized AuNPs was tested (see Figures S1 and S2 in SI). As shown in Figures S3 and S4 from SI, testing at the optimal salt concentration, in the presence of synthetic target, no increase or small increase in hydrodynamic diameter was observed by DLS measurements. However, in absence of synthetic targets substantial increases in hydrodynamic diameter was observed, from 80 to 254 nm for GNSp and from 71 to 233 nm for GNSh.

Transmission electron microscopy (TEM) images further supported these findings, showing more pronounced aggregation of gold nanospheres in the negative electrode group compared to that in the positive electrode group at optimal salt concentrations (see Figure S5 in SI). This differential aggregation behavior between the groups, along with distinct color changes over time, underscores the mitigating effect of target presence on NP aggregation, highlighting the potential for real-time detection applications.

Sensitivity and LOD of the Single AuNPs-Based Assay. The assay's limit of detection (LOD) was determined by conducting detection experiments with varying concentrations of synthetic targets for influenza A and SARS-CoV-2. The absorption ratios of these experiments with GNSp and GNSh, corresponding to different target concentrations, are depicted in Figure 3A and C, respectively. Both GNSp and

https://doi.org/10.1021/acsomega.4c04385
ACS Omega 2024, 9, 37163−37169

GNSh exhibited responses that were proportional to the concentration of the synthetic target, with absorption ratios containing synthetic target sequences higher than those of the negative control wells. Despite decreasing target concentrations, the absorption ratios remained higher than those of the negative control, enabling the detection of lower target concentrations. Specifically, the lowest detected concentrations were 33 nM for GNSp and 10 nM for GNSh.

Specificity of the Single AuNPs-Based Assay. To evaluate the specificity of GNSp and GNSh toward their respective complementary targets, each system was tested against noncomplementary targets. Figure 3B illustrates that when using GNSp, test wells containing water or SARS-CoV-2 targets became transparent, accompanied by a significant decrease in the absorbance at 538 nm. At the same time, wells containing influenza A target retained their red color, confirming the assay's specificity for influenza A. Similarly, with GNSh (Figure 3D), wells containing water or influenza A targets became transparent, with a notable decrease in absorbance at 616 nm, while wells containing SARS-CoV-2 targets retained a blue color, indicative of specific SARS-CoV-2 detection. These results demonstrate that in the presence of their complementary short targets, the probes on the AuNPs hybridize with them, resulting in the stabilization of the AuNP system against salt-induced aggregation. In the absence of a specific probe or in the presence of another short target sequence, no hybridization occurs, leading to AuNPs aggregation and subsequent transparency after the addition of salt due to salt-induced aggregation.

Testing the Hybrid System of GNSp and GNSh. In order to look at the multiplex ability of the system, we investigated the concurrent use of GNSp and GNSh as a hybrid system by mixing the two morphologies of gold nanoparticles. This hybrid system was then assessed for its ability to detect synthetic targets for SARS-CoV-2 and Influenza A, aiming to understand their interactions and assess their potential for dual identification. As illustrated in Figure 4A, dispersed GNSp exhibited a red color attributed to their plasmon resonance peak at 538 nm, while GNSh displayed a blue color due to their plasmon resonance at 616 nm. Upon their combination, the hybrid system exhibited a purple color, with a predominant peak at 546 nm. This slight shift in the plasmon resonance from 538 to 546 nm is attributed to the color mixing between the plasmon resonance of gold nanospheres at 538 nm and that of gold nanoshells at 616 nm.

Viral Short Target Sequence Analysis Based on the Hybrid System. Detection experiments were subsequently conducted utilizing the hybrid system, with UV−vis spectra in the presence or absence of synthetic targets depicted in Figure 4B. In the absence of the short target, the test transitioned well from purple to transparent. Upon introduction of the SARS-CoV-2 short target, the test well turned from purple to blue. With the UV−vis spectra revealing an absorption peak at 615 nm corresponding to the plasmon resonance of GNSh. Finally, in the presence of the influenza A synthetic target, the test well shifted from purple to indigo, and the UV−vis spectra exhibited a plasmon peak at 542 nm corresponding to the plasmon resonance of GNSp. Thus, the specific stabilization of AuNPs upon binding to their respective short targets facilitated the identification of the short target within the system based on the color of the assay or through UV−vis spectroscopy.

The outcomes demonstrated that when only one type of short target was introduced, AuNPs with their corresponding

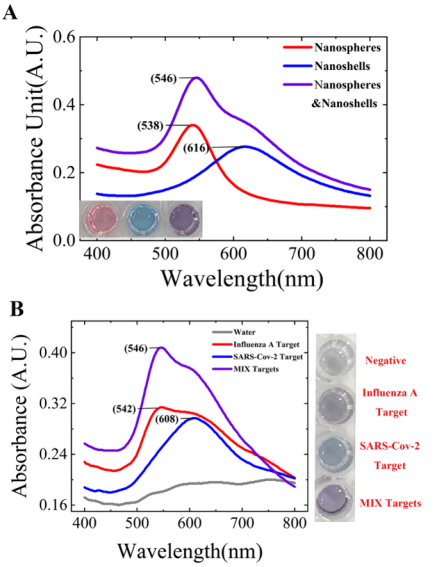

Figure 4. (A) UV−visible spectra and digital photograph of the GNSp, GNSh, and hybrid system. (B) UV−visible spectra and digital photograph of the virus short target sequence test of the hybrid system.

probes underwent hybridization, resulting in stability against salt-induced aggregation, while the other type of AuNPs aggregated under salt-induced conditions. Similarly, upon the addition of both short targets, AuNPs with their respective probes hybridized, and both types of AuNPs remained stable against salt-induced aggregation. In the absence of a specific probe, hybridization did not occur, leading to the aggregation of both types of AuNPs and subsequent transparency following the addition of salt.

Specificity and LOD Based on the Hybrid System Assay. To assess the specificity of the hybrid-system-based assay, several targets associated with other viruses (including Influenza B) were tested. Four types of targets were selected, and it was observed that these targets failed to stabilize the AuNPs in the hybrid system. UV−vis analysis clearly depicted a substantial decrease in the absorption of the plasmon resonance in the test wells containing influenza B targets, akin to the UV−vis spectrum observed in the negative control test wells, indicating nanoparticle aggregation (Figure 5) These spectrophotometric results confirmed the specificity of AuNPs detection using the hybrid system against both the influenza A virus and the SARS-CoV-2 virus.

To further validate and determine detection limits using the hybrid systems, different concentrations of the targets for the two viruses were tested. Absorption ratios (GNSp ratio = Abs_{538}/Abs_{750}, and GNSh ratio = Abs_{616}/Abs_{800}) were employed to assess the aggregation state of AuNPs. As illustrated in Figure 4B,C, the absorption ratio of the test wells containing the targets was higher than that of the negative control, indicating stabilization of the nanoparticles in the presence of the synthetic targets. The hybrid system responded to the synthetic target concentration with the absorption ratio decreasing as the short target concentration decreased. The lowest concentration of the short target detected for both systems was 100 nM.

https://doi.org/10.1021/acsomega.4c04385
ACS Omega 2024, 9, 37163−37169

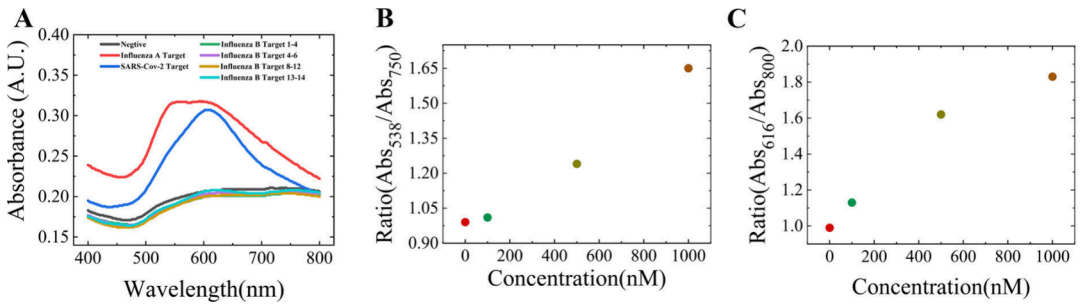

Figure 5. (A) Specificity study based on hybrid system analysis. (B) Hybrid system LOD testing for the target of influenza A virus (100, 500, and 1000 nM; ratio = Abs_{538}/Abs_{750}). (C) Hybrid system LOD testing for the target of SARS-CoV-2 virus (100, 500, and 1000 nM; ratio = Abs_{616}/Abs_{800}).

CONCLUSION

Two assays employing distinct nanoparticle shapes, gold nanospheres and gold nanoshells, were successfully developed. Functionalization of these nanoparticles with SARS-CoV-2 and Influenza A oligonucleotides was validated through UV−vis spectroscopy and DLS. Detection of synthetic SARS-CoV-2 and Influenza A targets was achieved with limits of detection of 10 and 33 nM, respectively, utilizing both nanoparticle systems.

Subsequently, two types of nanoparticles into a hybrid system capable of specifically identifying the presence of SARS-CoV-2 or influenza A targets were integrated. This hybrid approach facilitated the detection of both, with a limit of detection of 100 nM. Furthermore, the assay's specificity toward SARS-CoV-2 and Influenza A was verified by testing synthetic influenza B targets.

This innovative methodology presents a novel multiplexing strategy for rapid nucleic acid testing based on gold nanoparticle solutions. We envision further expansion of this approach to enable simultaneous multiplexing of a broader spectrum of diseases, leveraging the precise tuning of plasmon resonance in differently shaped nanoparticles such as gold nanorods. Compared to other methodologies employing nanostructures, and in particular gold NPs for sensing of viral DNA, our strategy enables detection of two diseases at the same time in a fast (∼20 min) and precise manner. Still our method relies on a UV−vis spectrophotometer readout, and to enhance the capabilities of our assay a portable reader or smartphone based app could be developed.

ASSOCIATED CONTENT

Supporting Information

The Supporting Information is available free of charge at https://pubs.acs.org/doi/10.1021/acsomega.4c04385.

The oligonucleotides and target sequences used in the experiments; The optimal salt concentration tests of GNSp and GNSh; Effect of the target on gold nanoparticle aggregation; TEM image of functionalized GNSp after reaction under optimal salt concentration conditions (PDF)

AUTHOR INFORMATION

Corresponding Authors

Lei Zhang − *Sino-Swiss Institute of Advanced Technology (SSIAT), Shanghai University, Shanghai 201899, China; School of Microelectronics, Shanghai University, Shanghai 201899, China*; Email: zhangleich@shu.edu.cn

Charles H. Lawrie − *Sino-Swiss Institute of Advanced Technology (SSIAT), Shanghai University, Shanghai 201899, China; Biogipuzkoa Health Research Institute, San Sebastian 20018, Spain; IKERBASQUE, Basque Foundation for Science, Bilbao E-48009, Spain; Radcliffe Department of Medicine, University of Oxford, Oxford OX1 4BH, United Kingdom*; orcid.org/0000-0002-8882-1131; Email: charles.lawrie@bio-gipuzkoa.eus

Authors

Shixi Zhang − *Sino-Swiss Institute of Advanced Technology (SSIAT), Shanghai University, Shanghai 201899, China; School of Microelectronics, Shanghai University, Shanghai 201899, China*

Yuhan Zhang − *Sino-Swiss Institute of Advanced Technology (SSIAT), Shanghai University, Shanghai 201899, China; School of Microelectronics, Shanghai University, Shanghai 201899, China*

Jiaye Jiang − *Sino-Swiss Institute of Advanced Technology (SSIAT), Shanghai University, Shanghai 201899, China; School of Microelectronics, Shanghai University, Shanghai 201899, China*

Mathias Charconnet − *Sino-Swiss Institute of Advanced Technology (SSIAT), Shanghai University, Shanghai 201899, China; School of Microelectronics, Shanghai University, Shanghai 201899, China*

Yuan Peng − *Sino-Swiss Institute of Advanced Technology (SSIAT), Shanghai University, Shanghai 201899, China; School of Microelectronics, Shanghai University, Shanghai 201899, China*

Complete contact information is available at: https://pubs.acs.org/10.1021/acsomega.4c04385

Author Contributions

The manuscript was written through the contributions of all authors. All authors have given approval to the final version of the manuscript. S.Z.: conceptualization, data curation, and writing the original draft. C.M.: conceptualization, data curation, writing, review, and editing. Y.Z.: data curation and formal analysis. J.J.: data curation and formal analysis. C.L.: conceptualization, supervision, funding acquisition, resources, review, and editing. L.Z.: conceptualization, supervision, funding acquisition, resources, review, and editing.

Notes

The authors declare no competing financial interest.

https://doi.org/10.1021/acsomega.4c04385
ACS Omega 2024, 9, 37163−37169

■ ACKNOWLEDGMENTS

The authors are grateful to Shanghai University for the support.

■ ABBREVIATIONS

ALP, alkaline phosphatase; AuNPs, gold nanoparticles; DLS, dynamic light scattering; EDTA, ethylene diamine tetraacetic acid; ELISA, enzyme-linked immunosorbent assay; GNSh, gold nanoshells; GNSp, gold nanospheres; LOD, limit of detection; PB, phosphate buffer; PCR, polymerase chain reaction; SDS, sodium dodecyl sulfate

■ REFERENCES

(1) Wang, M.; Yang, Y.; Min, J.; Song, Y.; Tu, J.; Mukasa, D.; Ye, C.; Xu, C.; Heflin, N.; McCune, J. S.; et al. A wearable electrochemical biosensor for the monitoring of metabolites and nutrients. *Nature Biomedical Engineering* **2022**, *6* (11), 1225−1235.

(2) Lu, L.; Zeng, R.; Lin, Q.; Huang, X.; Tang, D. Cation Exchange Reaction-Mediated Photothermal and Polarity-Switchable Photoelectrochemical Dual-Readout Biosensor. *Anal. Chem.* **2023**, *95* (44), 16335−16342.

(3) Santiago, I. Trends and Innovations in Biosensors for COVID-19 Mass Testing. *ChemBioChem.* **2020**, *21* (20), 2880−2889.

(4) Sanromán-Iglesias, M.; Garrido, V.; Gil-Ramírez, Y.; Aizpurua, J.; Grzelczak, M.; Grilló, M.-J. Plasmon-assisted fast colorimetric detection of bacterial nucleases in food samples. *Sens. Actuators, B* **2021**, *349*, 130780.

(5) Avni, T.; Leibovici, L.; Paul, M. PCR Diagnosis of Invasive Candidiasis: Systematic Review and Meta-Analysis. *Journal of Clinical Microbiology* **2011**, *49* (2), 665−670.

(6) Zafar, H.; Channa, A.; Jeoti, V.; Stojanović, G. M. Comprehensive Review on Wearable Sweat-Glucose Sensors for Continuous Glucose Monitoring. *Sensors* **2022**, *22*, 638.

(7) Clark, L. C., Jr; Lyons, C. Electrode Systems for Continuous Monitoring in Cardiovascular Surgery. *Ann. N.Y. Acad. Sci.* **1962**, *102* (1), 29−45.

(8) Velasco-Garcia, M. N.; Mottram, T. Biosensor Technology addressing Agricultural Problems. *Biosystems Engineering* **2003**, *84* (1), 1−12.

(9) Thakur, M. S.; Ragavan, K. V. Biosensors in food processing. *Journal of Food Science and Technology* **2013**, *50* (4), 625−641.

(10) Griesche, C.; Baeumner, A. J. Biosensors to support sustainable agriculture and food safety. *TrAC Trends in Analytical Chemistry* **2020**, *128*, 115906.

(11) Mohankumar, P.; Ajayan, J.; Mohanraj, T.; Yasodharan, R. Recent developments in biosensors for healthcare and biomedical applications: A review. *Measurement* **2021**, *167*, 108293.

(12) Liu, Q.; Wu, C.; Cai, H.; Hu, N.; Zhou, J.; Wang, P. Cell-Based Biosensors and Their Application in Biomedicine. *Chem. Rev.* **2014**, *114* (12), 6423−6461.

(13) Jain, A.; Homayoun, A.; Bannister, C. W.; Yum, K. Single-walled carbon nanotubes as near-infrared optical biosensors for life sciences and biomedicine. *Biotechnology Journal* **2015**, *10* (3), 447−459.

(14) Justino, C. I. L.; Duarte, A. C.; Rocha-Santos, T. A. P. Recent Progress in Biosensors for Environmental Monitoring: A Review. *Sensors* **2017**, *17*, 2918.

(15) Ejeian, F.; Etedali, P.; Mansouri-Tehrani, H.-A.; Soozanipour, A.; Low, Z.-X.; Asadnia, M.; Taheri-Kafrani, A.; Razmjou, A. Biosensors for wastewater monitoring: A review. *Biosens. Bioelectron.* **2018**, *118*, 66−79.

(16) Long, F.; Zhu, A.; Shi, H. Recent Advances in Optical Biosensors for Environmental Monitoring and Early Warning. *Sensors* **2013**, *13*, 13928−13948.

(17) Zhu, H.; Zhang, H.; Xu, Y.; Laššáková, S.; Korabečná, M.; Neužil, P. PCR past, present and future. *BioTechniques* **2020**, *69* (4), 317−325.

(18) Song, X.; Coulter, F. J.; Yang, M.; Smith, J. L.; Tafesse, F. G.; Messer, W. B.; Reif, J. H. A lyophilized colorimetric RT-LAMP test kit for rapid, low-cost, at-home molecular testing of SARS-CoV-2 and other pathogens. *Sci. Rep.* **2022**, *12* (1), 7043.

(19) López-Valls, M.; Escalona-Noguero, C.; Rodríguez-Díaz, C.; Pardo, D.; Castellanos, M.; Milán-Rois, P.; Martínez-Garay, C.; Coloma, R.; Abreu, M.; Cantón, R.; et al. CASCADE: Naked eye-detection of SARS-CoV-2 using Cas13a and gold nanoparticles. *Anal. Chim. Acta* **2022**, *1205*, 339749.

(20) Zeng, R.; Gong, H.; Li, Y.; Li, Y.; Lin, W.; Tang, D.; Knopp, D. CRISPR-Cas12a-Derived Photoelectrochemical Biosensor for Point-Of-Care Diagnosis of Nucleic Acid. *Anal. Chem.* **2022**, *94* (20), 7442−7448.

(21) Belza, J.; Opletalová, A.; Poláková, K. Carbon dots for virus detection and therapy. *Microchimica Acta* **2021**, *188* (12), 430.

(22) Elghanian, R.; Storhoff, J. J.; Mucic, R. C.; Letsinger, R. L.; Mirkin, C. A. Selective Colorimetric Detection of Polynucleotides Based on the Distance-Dependent Optical Properties of Gold Nanoparticles. *Science* **1997**, *277* (5329), 1078−1081.

(23) Gao, Z.; Qiu, Z.; Lu, M.; Shu, J.; Tang, D. Hybridization chain reaction-based colorimetric aptasensor of adenosine 5′-triphosphate on unmodified gold nanoparticles and two label-free hairpin probes. *Biosens. Bioelectron.* **2017**, *89*, 1006−1012.

(24) Zeng, R.; Qiu, M.; Wan, Q.; Huang, Z.; Liu, X.; Tang, D.; Knopp, D. Smartphone-Based Electrochemical Immunoassay for Point-of-Care Detection of SARS-CoV-2 Nucleocapsid Protein. *Anal. Chem.* **2022**, *94* (43), 15155−15161.

(25) Jauset-Rubio, M.; Svobodová, M.; Mairal, T.; McNeil, C.; Keegan, N.; Saeed, A.; Abbas, M. N.; El-Shahawi, M. S.; Bashammakh, A. S.; Alyoubi, A. O.; et al. Ultrasensitive, rapid and inexpensive detection of DNA using paper based lateral flow assay. *Sci. Rep.* **2016**, *6* (1), 37732.

(26) Borghei, Y.-S.; Samadikhah, H. R.; Hosseinkhani, S. Exploitation of N-Gene of SARS-CoV-2 to Develop a New Rapid Assay by ASOs@AuNPs. *Anal. Chem.* **2022**, *94* (39), 13616−13622.

(27) Alafeef, M.; Dighe, K.; Moitra, P.; Pan, D. Rapid, Ultrasensitive, and Quantitative Detection of SARS-CoV-2 Using Antisense Oligonucleotides Directed Electrochemical Biosensor Chip. *ACS Nano* **2020**, *14* (12), 17028−17045.

(28) Armesto, M.; Charconnet, M.; Marimón, J. M.; Fernández Regueiro, C. L.; Jia, J.; Yan, T.; Sorarrain, A.; Grzelczak, M.; Sanromán, M.; Vicente, M.; et al. Validation of Rapid and Economic Colorimetric Nanoparticle Assay for SARS-CoV-2 RNA Detection in Saliva and Nasopharyngeal Swabs. *Biosensors* **2023**, *13*, 275.

(29) Yoo, S. M.; Lee, S. Y. Optical Biosensors for the Detection of Pathogenic Microorganisms. *Trends Biotechnol.* **2016**, *34* (1), 7−25.

(30) Yassin, R.; Hanna, J.; El Bikai, R.; Mohtar, J.; El Chaar, M. Comparison of two commercial multiplex PCR assays for the detection of sexually transmitted infections. *Journal of Infection in Developing Countries* **2022**, *16* (02), 333−338.

(31) Lee, D.; Chu, C.-H.; Sarioglu, A. F. Point-of-Care Toolkit for Multiplex Molecular Diagnosis of SARS-CoV-2 and Influenza A and B Viruses. *ACS Sensors* **2021**, *6* (9), 3204−3213.

(32) Xu, Y.; Liu, Y.; Wu, Y.; Xia, X.; Liao, Y.; Li, Q. Fluorescent Probe-Based Lateral Flow Assay for Multiplex Nucleic Acid Detection. *Anal. Chem.* **2014**, *86* (12), 5611−5614.

(33) Lorenz, R.; Bernhart, S. H.; Höner zu Siederdissen, C.; Tafer, H.; Flamm, C.; Stadler, P. F.; Hofacker, I. L. ViennaRNA Package 2.0. *Algorithms for Molecular Biology* **2011**, *6* (1), 26.

(34) Abavisani, M.; Rahimian, K.; Mahdavi, B.; Tokhanbigli, S.; Mollapour Siasakht, M.; Farhadi, A.; Kodori, M.; Mahmanzar, M.; Meshkat, Z. Mutations in SARS-CoV-2 structural proteins: a global analysis. *Virology Journal* **2022**, *19* (1), 220.

(35) Farhud, D. D.; Mojahed, N. SARS-COV-2 Notable Mutations and Variants: A Review Article. *Iranian journal of public health* **2022**, *51* (7), 1494−1501.

(36) Farhud, D. D.; Mojahed, N. SARS-COV-2 Notable Mutations and Variants: A Review Article. *Iranian Journal of Public Health* **2022**, *51* (7), 1494.

https://doi.org/10.1021/acsomega.4c04385
ACS Omega 2024, 9, 37163−37169